https://doi.org/10.5194/egusphere-2024-1118
Preprint. Discussion started: 24 May 2024

Coupling the urban canopy model TEB (SURFEXv9.0) with the radiation model SPARTACUS-Urbanv0.6.1 for more realistic urban radiative exchange calculation

Robert Schoetter[1], Robin James Hogan[2,3], Cyril Caliot[4], and Valéry Masson[1]

[1]CNRM, Université de Toulouse, Météo-France, CNRS, 42 avenue Gaspard Coriolis, Toulouse, France
[2]ECMWF, Reading, United Kingdom
[3]Department of Meteorology, University of Reading, United Kingdom
[4]CNRS, UPPA, E2S, LMAP, 1 Allée du Parc Montaury, Anglet, France

Correspondence: Robert Schoetter (robert.schoetter@meteo.fr)

Abstract. The urban canopy model TEB is coupled with the radiation model SPARTACUS-Urban to improve both the urban geometry simplification and radiative transfer calculation. SPARTACUS-Urban assumes that the probability density function of wall-to-wall and ground-to-wall distances follows a decreasing exponential. This matches better the distributions in real cities compared to the infinitely-long street canyon employed by the classical TEB. SPARTACUS-Urban solves the radiative transfer equation using the discrete ordinate method. This allows to take into account physical processes like the interaction of radiation with air in the urban canopy layer, spectral dependency of urban material reflectivities, or specular reflections. Such processes would be more difficult to account for with the radiosity method used by the classical TEB. With SPARTACUS-Urban, the mean radiant temperature, a crucial parameter for outdoor human thermal comfort, can be calculated using the radiative fluxes in vertical and horizontal direction incident on a human body in the urban environment. TEB-SPARTACUS is validated by comparing the solar and terrestrial urban radiation budget observables with those simulated by the Monte-Carlo-based HTRDR-Urban reference model for procedurally-generated urban districts mimicking the Local Climate Zones. An improvement is found for almost all radiative observables and urban morphologies for direct solar, diffuse solar, and terrestrial infrared radiation. TEB-SPARTACUS might therefore lead to more realistic results for building energy consumption, outdoor human thermal comfort, or the urban heat island effect.

1 Introduction

Radiative exchange is a crucial physical process for the urban climate. Multiple reflections of solar radiation in the 3-D urban geometry lead to a lower effective reflectivity (albedo) of a city compared to a flat surface (Krayenhoff et al., 2014). In the nighttime, downwelling terrestrial infrared radiation at the surface is higher in urban areas compared to open rural areas, which is due to the infrared radiation emission towards the ground from buildings or urban trees with a higher surface temperature than the sky radiative temperature. Radiative exchange contributes to the higher (nocturnal) air temperature in urban areas compared to the surrounding rural areas (the urban heat island effect, Oke (1982)), although it is not its main cause. Shading and multiple reflection of radiation by complex building and vegetation geometries change the radiation received by buildings

https://doi.org/10.5194/egusphere-2024-1118
Preprint. Discussion started: 24 May 2024

and humans in the urban environment compared to an open rural environment. This is relevant for building energy consumption (Strømann-Andersen and Sattrup, 2011; Frayssinet et al., 2018), and human thermal comfort (Fröhlich and Matzarakis, 2020; Dissegna et al., 2021; Geletič et al., 2022).

Urban canopy models (UCMs) like the Town Energy Balance (TEB, Masson (2000)) or the Building Effect Parametrisation (BEP, Martilli et al. (2002)) that calculate the urban surface energy balance in mesoscale or global atmospheric models (Grimmond et al., 2010, 2011) strongly simplify both urban geometry and radiative transfer physics. The most frequently-used UCM geometry is the infinitely-long street canyon; the radiosity method is common for radiative exchange calculation (Schoetter et al., 2023). It assumes that radiation is reflected isotropically (Lambertian surfaces), that there is vacuum in between the buildings, and that there is no wavelength-dependency of material reflectivity (broadband materials).

Hogan (2019a) found that radiative transfer in the urban canopy layer (UCL) is governed by the probability density functions of wall-to-wall (p_{ww}) and ground-to-wall (p_{gw}) distances since these determine the probability that radiation travelling through the UCL is intercepted by buildings or the ground. Hogan (2019a) and Stretton et al. (2022) investigated p_{ww} and p_{gw} for districts in real cities and found systematic differences between them and the distribution that is implicitly assumed when using the infinitely-long street canyon geometry. This leads to wrong mean rates of solar and thermal infrared radiation exchange between the sky, walls, and ground. Instead, a decreasing exponential function fits better the p_{ww} and p_{gw} in real cities. For urban districts in which this decreasing exponential function of p_{ww} and p_{gw} holds, the attenuation of radiation by buildings can be described using the Beer-Lambert law in the same way as for radiation travelling through the turbid atmosphere.

In light of these findings, Hogan (2019b) adapted the SPARTACUS (SPeedy Algorithm for Radiative TrAnsfer through CloUd Sides; Schäfer et al. (2016), Hogan et al. (2016)) atmospheric radiation model representing the 3-D radiative interactions between clouds to the UCL (SPARTACUS-Urban). SPARTACUS-Urban is part of the land surface radiation model SPARTACUS-Surface. It relies on the 1-D discrete ordinate method and divides the UCL into the built, the urban tree, and the clear-air region. In the vertical direction, SPARTACUS-Urban can divide the urban canopy into multiple layers, which allows to take into account a variety of building and tree heights at each grid point. It can represent physical processes like specular reflections, or interaction of radiation with air, aerosols, or clouds in the UCL which are difficult to account for with the radiosity method. It can also more realistically account for the interaction of radiation with trees, because it represents them as cylinders thus conserving their contact area with air and buildings.

Hogan (2019b) validated SPARTACUS-Urban with Monte-Carlo reference simulations for the particular case of forest sites without buildings. Stretton et al. (2022) evaluated the solar radiation budget simulated by SPARTACUS-Urban for urban geometries of different complexity including real cities with simulations employing the obstacle-resolving radiation model Discrete Anisotropic Radiative Transfer (DART; Gastellu-Etchegorry (2008); Gastellu-Etchegorry et al. (2015)). They find a very good performance of SPARTACUS-Urban as long as the assumption of the decreasing exponential function for p_{ww} and p_{gw} holds. Otherwise, larger biases appear, but the overall performance is still good. Stretton et al. (2023) evaluated SPARTACUS-Urban against DART for terrestrial radiation in a central London domain for both homogeneous and heterogeneous skin surface temperature of urban facets.

Coupling SPARTACUS-Urban with UCMs is promising to improve the realism of urban geometry and radiative transfer physics

https://doi.org/10.5194/egusphere-2024-1118
Preprint. Discussion started: 24 May 2024

in these models. Furthermore, the benefits of some adaptation measures to climate change (e.g. street trees or construction materials with specific spectral reflectivities) can be better quantified with SPARTACUS-Urban. This study presents the coupling of SPARTACUS-Urban with the UCM TEB (TEB-SPARTACUS). TEB is used to simulate the urban surface energy balance as a function of the meteorological conditions at the top of the urban roughness sublayer (2-5 times the characteristic building height, Roth (2000)). The original TEB, hereafter TEB-Classical, represents the city as an infinitely-long street canyon. It solves the energy budget separately for the roof, the walls, and the ground. TEB can solve the 1-D prognostic equations of wind speed, air temperature, humidity, and turbulence kinetic energy for the air in the UCL (surface boundary layer scheme SBL) (Hamdi and Masson, 2008). In-canyon vegetation on the ground has been added by Lemonsu et al. (2012), vertically-extended in-canyon vegetation by Redon et al. (2017, 2020). The urban trees are represented by a turbid layer filling the entire street canyon between trunk and tree height. A building energy model (Bueno et al. (2012), Pigeon et al. (2014)) solves the energy budget of a representative building at district scale taking into account human behaviour related to building energy consumption (Schoetter et al., 2017). TEB is used as lower boundary condition for cities in mesoscale atmospheric models like Meso-NH (Lac et al., 2018), Numerical Weather Prediction models like AROME (Seity et al., 2011), or regional climate models like CNRM-ALADIN (Daniel et al., 2019), and CNRM-AROME (Lemonsu et al., 2023).

This study is structured as follows. The technical aspects of the coupling between TEB and SPARTACUS-Urban are described in Section 2, the methodology for the TEB-SPARTACUS validation in Section 3, and the validation results in Section 4. Conclusions are drawn in Section 5.

2 Technical aspects of the TEB and SPARTACUS-Urban coupling

2.1 TEB-SPARTACUS geometry

The original TEB (Masson, 2000) is a single-layer UCM. This means that the building roof is at the surface level of the atmospheric model; the walls and the road are below surface level. Schoetter et al. (2020) added the option to couple TEB at multiple levels with the atmospheric model; the buildings are immersed in the atmosphere with the multi-layer TEB. With both the single- and multi-layer TEB, there is only one average building (H_{build}) and tree (H_{tree}) height at each grid point. Furthermore, the radiation received and absorbed by the building walls and the trees is calculated on one single node; no vertical discretisation is made. TEB-SPARTACUS would allow to take into account a variety of building and tree heights at each grid point, and to calculate a vertical profile of the radiation received and absorbed by the walls. However, this would require to modify the input parameters of SURFEX-TEB and also other physical routines, which is left to future developments. In this article, except for the assumption of the decreasing exponential function for p_{ww} and p_{gw} inherent to SPARTACUS-Urban, the geometrical complexity of TEB is not changed.

https://doi.org/10.5194/egusphere-2024-1118
Preprint. Discussion started: 24 May 2024

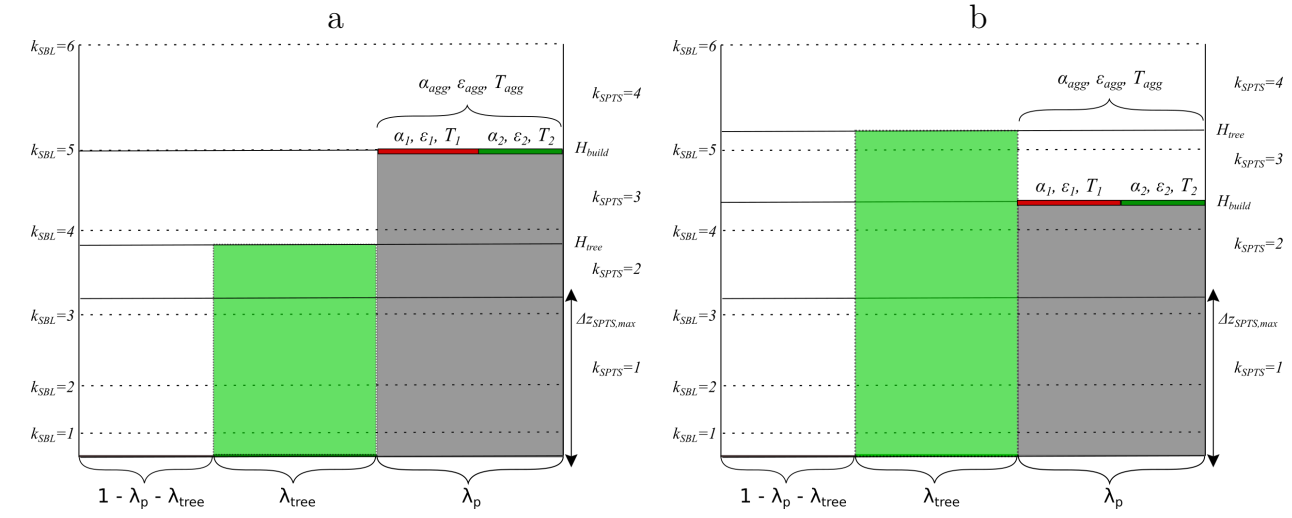

Figure 1. TEB-SPARTACUS vertical levels for (a): a grid point with the buildings (grey) higher than the trees (green) ($H_{\mathrm{build}} > H_{\mathrm{tree}}$) and (b): a grid point with the buildings lower than the trees ($H_{\mathrm{build}} < H_{\mathrm{tree}}$). The k_{SBL} display the center of the TEB Surface Boundary Layer (SBL) mass levels, the k_{SPTS} the TEB-SPARTACUS vertical levels. Urban facet properties like albedo (α), emissivity (ϵ), and skin surface temperature (T) that might exhibit an intra-facet variety in TEB (e.g. due to a part of the roofs covered by green roofs (de Munck et al., 2013)) are aggregated before their use in SPARTACUS-Urban. The x-axis represents the horizontal extent of buildings (λ_p), urban trees (λ_{tree}), and clear air ($1 - \lambda_p - \lambda_{\mathrm{tree}}$) in the urban canopy layer.

2.2 TEB-SPARTACUS vertical levels

The TEB-SPARTACUS vertical levels are set as a function of H_{build} and H_{tree} such that one level is either entirely vertically intersected by trees and/or buildings, or entirely free of them (Figure 1). With this approach it is not necessary to vertically interpolate the geometrical parameters of buildings and trees, which could lead to physical inconsistancies. For a grid point with $H_{\mathrm{build}} > H_{\mathrm{tree}}$, vertical levels with a maximum height of $\Delta_{\mathrm{sps,max}}$ are defined from the ground to H_{tree}. These contain a built, tree, and clear-air region. Above H_{tree}, one or several levels of maximum height $\Delta_{\mathrm{sps,max}}$ are placed until H_{build} is reached. These levels contain only buildings and clear air. One layer of clear air is placed above the buildings for numerical reasons. For a grid point with $H_{\mathrm{build}} < H_{\mathrm{tree}}$, the TEB-SPARTACUS vertical levels are set in a similar way. The default value of $\Delta_{\mathrm{sps,max}}$ is 1 m.

2.3 TEB-SPARTACUS input parameters

The TEB-SPARTACUS input parameters are listed in Table 1. Some of these parameters are exactly the same as in TEB. This is indicated by "TEB variable" in Table 1. However, SPARTACUS-Urban requires some input parameters that are not present in TEB; these have to be calculated based on the TEB variables or specified, which is explained in the following. The

https://doi.org/10.5194/egusphere-2024-1118
Preprint. Discussion started: 24 May 2024

characteristic building diameter D is calculated assuming cylindrical buildings (Eq. 3) by combining the equations defining the plane area building density (λ_p; Eq. 1) and the external wall surface density (λ_w; Eq. 2).

$$\lambda_p = \frac{\pi D^2}{4A_{\text{ref}}} \tag{1}$$

$$\lambda_w = \frac{\pi D H_{\text{build}}}{A_{\text{ref}}} \tag{2}$$

$$D = \frac{4\lambda_p H_{\text{build}}}{\lambda_w} \tag{3}$$

A_{ref} is the surface area of the grid point.

The TEB SBL levels might be different from those of TEB-SPARTACUS (Figure 1). The air temperature values from the SBL vertical levels are linearly interpolated on the center of the TEB-SPARTACUS vertical levels.

TEB can take into account a variety of surface covers per type of urban facet. The building roofs can be covered by the native building roof external cover, snow, solar panels (Masson et al., 2014), or green roofs (de Munck et al., 2013). The ground can be covered by roads, bare ground, low vegetation, or snow. The building walls consist of the wall external material and potentially windows. To keep the SPARTACUS-Urban code independent of its use by TEB, it uses aggregated radiative properties for each facet. After the call of SPARTACUS-Urban, the radiation absorbed by the different surface covers is calculated. Considering a facet consisting of two surface covers (an example for the roof is displayed in Figure 1) with fractional cover f_1 and f_2, albedos α_1 and α_2, emissivities ϵ_1 and ϵ_2, and surface temperatures T_1 and T_2, the aggregated values of albedo (α_{agg}), emissivity (ϵ_{agg}), and radiative surface temperature (T_{agg}) used by SPARTACUS-Urban are calculated as follows:

$$\alpha_{\text{agg}} = \frac{f_1\alpha_1 + f_2\alpha_2}{f_1 + f_2} \tag{4}$$

$$\epsilon_{\text{agg}} = \frac{f_1\epsilon_1 + f_2\epsilon_2}{f_1 + f_2} \tag{5}$$

$$T_{\text{agg}} = \frac{f_1\epsilon_1\sigma {T_1}^4 + f_2\epsilon_2\sigma {T_2}^4}{(f_1 + f_2)\sigma\epsilon_{\text{agg}}} \tag{6}$$

SPARTACUS-Urban calculates the average solar (SW_{inc}) and infrared (LW_{inc}) radiation incident on a facet. The solar (SW_{abs}) and infrared (LW_{abs}) radiation absorbed by the two surface covers is calculated following

$$\text{SW}_{\text{abs},1} = (1-\alpha_1)\text{SW}_{\text{inc}} \quad \text{SW}_{\text{abs},2} = (1-\alpha_2)\text{SW}_{\text{inc}} \tag{7}$$

$$\text{LW}_{\text{abs},1} = \epsilon_1(\text{LW}_{\text{inc}} - \sigma {T_1}^4) \quad \text{LW}_{\text{abs},2} = \epsilon_2(\text{LW}_{\text{inc}} - \sigma {T_2}^4) \tag{8}$$

https://doi.org/10.5194/egusphere-2024-1118
Preprint. Discussion started: 24 May 2024

SPARTACUS-Urban represents the radiative exchanges between trees, walls, and the clear-air with more detail than TEB, taking into account a more realistic shape of trees with a characteristic diameter D_{tree}, and a potential variability of the optical depth of trees ($\mathrm{FSD}_{\mathrm{tree}}$). These parameters are currently specified in the code; future work could investigate whether it would be possible to link them to physiographic input variables (like the surface cover) or to specify them via databases. The fraction of tree surface in contact with walls ($\mathrm{FC}_{\mathrm{tree}}$) is calculated based on the tree surface cover fraction (λ_{tree}) assuming a random positioning of trees in the urban canyon following

$$\mathrm{FC}_{\mathrm{tree}} = \frac{\lambda_{\mathrm{tree}}}{1-\lambda_p} \tag{9}$$

The air temperature in the vegetation canopy ($T_{\mathrm{air,veg}}$) is assumed to be equal to the air temperature in the clear-air region (T_{air}). SPARTACUS-Urban allows to consider scattering and absorption of solar radiation in the urban canopy. This is specified via the extinction coefficients ($k_{\mathrm{ext,air,sw}}$, $k_{\mathrm{kext,air,lw}}$) and the single scattering albedo of air for solar ($\alpha_{\mathrm{ssa,air,sw}}$) and terrestrial radiation ($\alpha_{\mathrm{ssa,air,lw}}$). These coefficients are currently set to 0, but could be calculated as a function of air temperature, humidity, liquid water content, and aerosol concentration by coupling with an atmospheric radiation scheme.

The single-scattering albedo for solar radiation of a leave ($\alpha_{\mathrm{ssa,tree,sw}}$) is assumed to be 0.4, which corresponds to a value integrated over the solar spectrum. This is different from the bulk vegetation albedo in the original TEB, because this parameter corresponds to an effective albedo after multiple reflections. The single scattering albedo for terrestrial radiation of a leave ($\alpha_{\mathrm{ssa,tree,lw}}$) is calculated based on the value of the tree emissivity (ϵ_{tree}) in TEB following

$$\alpha_{\mathrm{ssa,tree,lw}} = 1 - \epsilon_{\mathrm{tree}} \tag{10}$$

The tree extinction coefficient ($k_{\mathrm{ext,tree}}$) is calculated based on the vertical profile of Leaf Area Density (LAD) assuming isotropical leave orientation:

$$k_{\mathrm{ext,tree}} = 0.5\mathrm{LAD} \tag{11}$$

SPARTACUS-Urban allows to take into account the fraction of specular reflections from the walls ($f_{\mathrm{ref,specular}}$). It is set to 0 here, but could be linked to the glazing ratio and characteristics of wall and window materials.

https://doi.org/10.5194/egusphere-2024-1118
Preprint. Discussion started: 24 May 2024

Table 1. Input parameters for SPARTACUS-Urban when called by TEB.

Symbol	Parameter	Unit	Provenance
α_{agg}	Aggregated albedo of roof, wall, ground	1	Eq. 4
$\alpha_{\mathrm{ssa,air,lw}}$	Single-scattering albedo of terrestrial radiation with air	1	Set to 0
$\alpha_{\mathrm{ssa,air,sw}}$	Single-scattering albedo of solar radiation with air	1	Set to 0
$\alpha_{\mathrm{ssa,tree,lw}}$	Single-scattering albedo of terrestrial radiation with a leave	1	Eq. 10
$\alpha_{\mathrm{ssa,tree,sw}}$	Single-scattering albedo of solar radiation with a leave	1	Set to 0.4
D	Characteristic building diameter	m	Eq. 3
D_{tree}	Characteristic tree diameter	m	Set to 5 m
ϵ_{agg}	Aggregated emissivity of roof, wall, ground	1	Eq. 5
$f_{\mathrm{ref,specular}}$	Fraction of specular reflections from the walls	1	Set to 0
FC_{tree}	Fraction of trees in contact with walls	1	Eq. 9
$\mathrm{FSD}_{\mathrm{tree}}$	Fractional standard deviation of tree optical depth	1	Set to 0
$k_{\mathrm{ext,air,lw}}$	Terrestrial radiation extinction coefficient of air	m^{-1}	Set to 0
$k_{\mathrm{ext,air,sw}}$	Solar radiation extinction coefficient of air	m^{-1}	Set to 0
$k_{\mathrm{ext,tree}}$	Extinction coefficient of urban trees	m^{-1}	Eq. 11
λ_p	Plane area building density	1	TEB variable
λ_{tree}	Plane area tree density	1	TEB variable
T_{agg}	Aggregated skin surface temperature of roof, wall, ground	K	Eq. 6
T_{air}	Temperature of the clear-air region	K	Interpolated from TEB SBL levels
$T_{\mathrm{air,veg}}$	Air temperature of the vegetation region	K	Equal to T_{air}
$T_{\mathrm{surf,tree}}$	Skin surface temperature of the leaves	K	TEB variable

https://doi.org/10.5194/egusphere-2024-1118
Preprint. Discussion started: 24 May 2024

Table 2. Output parameters of SPARTACUS-Urban used by TEB.

Symbol	Parameter	Unit	Destination
$\alpha_{\mathrm{town,diff,sw}}$	Diffuse solar albedo of city	1	Coupling with atmospheric model
$\alpha_{\mathrm{town,dir,sw}}$	Direct solar albedo of city	1	Coupling with atmospheric model
$\mathrm{frac}_{\mathrm{gr,sunlit}}$	Fraction of sunlit ground	1	Diagnostic for human thermal comfort quantification
$\mathrm{LW}_{\mathrm{abs}}$	Terrestrial radiation absorbed by urban facet	Wm^{-2}	TEB prognostic equation of facet temperature
$\mathrm{LW}_{\mathrm{down,gr}}$	Downwelling terrestrial radiation at ground level	Wm^{-2}	Calculation of MRT (Eq. 12)
$\mathrm{LW}_{\mathrm{hor,diff,gr}}$	Terrestrial radiation at ground level on vertical plane	Wm^{-2}	Calculation of MRT (Eq. 12)
$\mathrm{LW}_{\mathrm{inc}}$	Terrestrial radiation incident on urban facet	Wm^{-2}	TEB prognostic equation of facet temperature
$\mathrm{LW}_{\mathrm{up,gr}}$	Upwelling terrestrial radiation at ground level	Wm^{-2}	Calculation of MRT (Eq. 12)
$\mathrm{SW}_{\mathrm{abs}}$	Solar radiation absorbed by urban facet	Wm^{-2}	TEB prognostic equations of facet temperature
$\mathrm{SW}_{\mathrm{down,diff,gr}}$	Downwelling diffuse solar radiation at ground level	Wm^{-2}	Calculation of MRT (Eq. 12)
$\mathrm{SW}_{\mathrm{down,dir,gr}}$	Downwelling direct solar radiation at ground level	Wm^{-2}	Calculation of MRT (Eq. 14)
$\mathrm{SW}_{\mathrm{hor,diff,gr}}$	Diffuse solar radiation at ground level on vertical plane	Wm^{-2}	Calculation of MRT (Eq. 12)
$\mathrm{SW}_{\mathrm{inc}}$	Solar radiation incident on urban facet	Wm^{-2}	TEB prognostic equation of facet temperature
$\mathrm{SW}_{\mathrm{up,diff,gr}}$	Upwelling diffuse solar radiation at ground level	Wm^{-2}	Calculation of MRT (Eq. 12)

https://doi.org/10.5194/egusphere-2024-1118
Preprint. Discussion started: 24 May 2024

2.4 Calculation of the Mean Radiant Temperature

The Mean Radiant Temperature (MRT) is a crucial input parameter for outdoor human thermal comfort indices like the Universal Thermal Climate Index (UTCI, Blazejczyk et al. (2012)). With the original TEB radiation scheme, it is calculated via the radiosity method using the shape factors between the human body and the different urban facets (road, walls, windows, and vegetation); the detailed equations are given in the supplementary material of Kwok et al. (2019). With TEB-SPARTACUS, the MRT is calculated differently. The flux densities of diffuse solar and infrared up- and downwelling radiation ($\mathrm{SW}_{\mathrm{up,diff,gr}}$, $\mathrm{SW}_{\mathrm{down,diff,gr}}$, $\mathrm{LW}_{\mathrm{up,gr}}$, $\mathrm{LW}_{\mathrm{down,gr}}$) at ground level are known. Furthermore, the diffuse solar and terrestrial fluxes incident on a vertical plane at ground level ($\mathrm{SW}_{\mathrm{hor,diff,gr}}$, $\mathrm{LW}_{\mathrm{hor,gr}}$) can be diagnosed with TEB-SPARTACUS. The fluxes in vertical and horizontal directions are weighted following Thorsson et al. (2007) to obtain the average diffuse radiative flux density absorbed by the human body:

$$R_{\mathrm{bd,diff}} = (1-\alpha_{\mathrm{bd}})\,(0.88\ \mathrm{SW}_{\mathrm{hor,diff,gr}} + 0.06\ \mathrm{SW}_{\mathrm{up,diff,gr}} + 0.06\ \mathrm{SW}_{\mathrm{down,diff,gr}}) \\ +\epsilon_{\mathrm{bd}}\,(0.88\ \mathrm{LW}_{\mathrm{hor,gr}} + 0.06\ \mathrm{LW}_{\mathrm{up,gr}} + 0.06\ \mathrm{LW}_{\mathrm{down,gr}}) \tag{12}$$

with α_{bd} (0.3) and ϵ_{bd} (0.97) the albedo and emissivity of the human body, respectively. The fluxes in the horizontal direction have a higher weight than the fluxes in the vertical direction, because the human body is considered to be in an upright position. The average total (diffuse and direct) radiative flux density absorbed by the human body when exposed entirely to the solar radiation is calculated following

$$R_{\mathrm{bd,sun}} = R_{\mathrm{bd,diff}} + (1-\alpha_{\mathrm{bd}})\mathrm{SW}_{\mathrm{dir,bd}} \tag{13}$$

with the average direct solar radiative flux density incident on the human body ($\mathrm{SW}_{\mathrm{dir,bd}}$) given by

$$\mathrm{SW}_{\mathrm{dir,bd}} = 0.308\frac{\mathrm{SW}_{\mathrm{down,dir,gr}}}{max(0.05, sin(\beta))}cos\left(\beta(1-\frac{\beta^2}{14.744})\right) \tag{14}$$

$\mathrm{SW}_{\mathrm{down,dir,gr}}$ is the direct solar radiation reaching the ground and β is the solar elevation angle. Based on these fluxes, the MRT for a human body exposed to only diffuse solar radiation ($\mathrm{MRT}_{\mathrm{shade}}$) and a human body entirely exposed to the direct solar radiation ($\mathrm{MRT}_{\mathrm{sun}}$) are then calculated following

$$\mathrm{MRT}_{\mathrm{sun}} = \left(\frac{R_{\mathrm{bd,sun}}}{\epsilon_{\mathrm{bd}}\sigma}\right)^{0.25} \tag{15}$$

$$\mathrm{MRT}_{\mathrm{shade}} = \left(\frac{R_{\mathrm{bd,diff}}}{\epsilon_{\mathrm{bd}}\sigma}\right)^{0.25} \tag{16}$$

The radiative fluxes are taken at ground level whereas it would be a bit more precise to calculate them at $1\ \mathrm{m}$ above ground, because this would better represent their average effect on the human body. The difference of the fluxes between the ground level and $1\ \mathrm{m}$ above ground is currently neglected. By taking into account the fluxes from vertical building walls, TEB-SPARTACUS allows for a more realistic estimation of MRT in urban areas from weather models and reanalysis data than previous work considering only flat ground (Di Napoli et al., 2020).

https://doi.org/10.5194/egusphere-2024-1118
Preprint. Discussion started: 24 May 2024

3 Methodology for TEB-SPARTACUS validation

Validation of TEB-SPARTACUS with observations of radiative and turbulent fluxes in real cities like those presented by Lipson et al. (2022) is not a promising strategy since the differences between the simulated and observed fluxes can be due to differences in the urban morphology, building construction material parameters, or anthropogenic heat fluxes between the real city and the simplified representation of the city in TEB. Furthermore, observations are uncertain themselves. It would therefore be difficult to attribute a potential improvement of the fluxes simulated with TEB-SPARTACUS to the better representation of urban geometry or radiative transfer physics. For this reason, in this study, the radiative observables simulated by TEB are evaluated with the Monte-Carlo-based HTRDR-Urban reference model (Caliot et al., 2022).

3.1 HTRDR-Urban reference model of urban radiative transfer

HTRDR-Urban uses a backward Monte-Carlo algorithm with the null-collision technique (Galtier et al., 2013; El Hafi et al., 2021) and accelerating grids (Villefranque et al., 2019) to solve the Radiative Transfer Equation (RTE) for solar and terrestrial radiation. It takes into account the interaction between radiation and the atmosphere with non-grey absorption, emission, and anisotropic scattering. 3-D absorption and scattering coefficient data as well as scattering phase functions characterise the spectral and directional radiative properties of gases, liquid droplets, and solid particles. At the Top Of Atmosphere (TOA), the observed solar spectrum irradiance averaged for 2020 from Coddington et al. (2015) is prescribed. At the Earth's surface, opaque surfaces consisting of vegetation and buildings described via triangles in a wavefront (.obj) file are prescribed. They can be specular or Lambertian reflectors, with a potentially wavelength-dependent reflectivity. Measured spectral Lambertian reflectivities contained in the Spectral Library of impervious Urban Materials (SLUM) available from the London Urban Micromet data Archive (LUMA) (Kotthaus et al., 2013, 2014) are distributed with HTRDR-Urban. A constant surface temperature is assigned to the surface triangles.

3.2 Procedurally-generated urban morphologies

Exactly the same urban morphologies as described in Section 4 of Schoetter et al. (2023) and displayed in Table 3 of Schoetter et al. (2023) are investigated. They have been created with a procedural city generator, their spatial extent is $800\ \mathrm{m}$ x $800\ \mathrm{m}$, and they mimick homogeneous urban districts covered by one type of Local Climate Zone (LCZ; Stewart and Oke (2012)). For each morphology, a representative street canyon with the same λ_p, λ_w, and mean building height (H_{mean}) that the actual morphology is created. Potential overhanging roofs that may occur in real cities are not considered. Schoetter et al. (2023) investigated the p_{ww} and p_{gw} for the procedurally-generated morphologies and found a good agreement with the decreasing exponential function.

A copy of the LCZ2a, LCZ4, LCZ5, and LCZ9 morphologies with trees represented by trunks, branches, and individual leaves is created. All trees are of the same height ($10\ \mathrm{m}$), diameter ($10.55\ \mathrm{m}$), and leaf area index ($\mathrm{LAI} = 2.24$). Since the trees do not intersect the buildings, more trees can be placed in the low density morphologies than in the high density ones. There are

https://doi.org/10.5194/egusphere-2024-1118
Preprint. Discussion started: 24 May 2024

64 trees for LCZ2a, 963 for LCZ4, 869 for LCZ5, and 1045 for LCZ9. The values of λ_{tree} are 0.01 for LCZ2a, 0.13 for LCZ4, 0.12 for LCZ5, and 0.14 for LCZ9, respectively.

3.3 Radiative boundary conditions

The UCL solar radiation budget consists of the downwelling and reflected solar radiation flux densities at the top of the UCL ($\dot{Q}_D$ and $\dot{Q}_U$), the flux density absorbed by the roofs ($\dot{Q}_R$), the walls including the windows ($\dot{Q}_W$), the ground ($\dot{Q}_G$), the urban trees ($\dot{Q}_T$), and the air ($\dot{Q}_{\text{air}}$). The UCL terrestrial radiation budget consists of the terrestrial radiation exchanged (absorbed minus emitted) by the sky, the roofs, the walls including the windows, the ground, the trees, and the air ($\dot{E}_{\text{sky}}$, $\dot{E}_R$, $\dot{E}_W$, $\dot{E}_G$, $\dot{E}_T$, and $\dot{E}_{\text{air}}$). In this study, vacuum radiative properties are assumed for the air in the UCL, therefore $\dot{Q}_{\text{air}} = 0$ and $\dot{E}_{\text{air}} = 0$. The following boundary conditions for downwelling radiation are considered:

- Purely direct downwelling solar radiation at the top of the UCL is achieved by setting the atmospheric radiative properties to those of vacuum. As a result, there is no downwelling scattered radiation at the UCL top. Simulations are made for solar elevation angles (γ) of 1°, 5°, 10°, 20°, 30°, 45°, 60°, 75°, and 90°. No specific solar azimuth is considered; for each Monte-Carlo realisation, the solar azimuth angle is randomly sampled with a uniform distribution between 0° and 360°. Schoetter et al. (2023) found that the number of Monte-Carlo realisations (N) needs to be larger for lower values of γ than for higher ones to achieve a given accurracy of the radiative observables. For this reason, N is specified following

$$N_\gamma = \text{int}\left(\frac{N_{\text{zen}}}{\sin(\gamma)}\right). \tag{17}$$

  The number of Monte-Carlo realisations for $\gamma = 90°$ (zenith) is $N_{\text{zen}} = 10^6$. int denotes rounding to nearest integer.

- Purely diffuse downwelling solar radiation at the top of the UCL is achieved by setting the atmospheric radiative properties to vacuum ones and prescribing a sky model with isotropic downwelling solar radiation leading to a flux density of $\dot{Q}_D = 1\ \text{W m}^{-2}$.

- For the terrestrial radiation simulations, a 1-D atmospheric profile consisting of mid-latitude summer (MLS) conditions is employed. For this profile, the near-surface air temperature is 294.2 K.

3.4 Numerical tests and uncertainty quantification

The following numerical tests are made:

- For the urban geometries without trees, simulations with HTRDR-Urban, TEB-Classical, and TEB-SPARTACUS are made for direct and diffuse solar radiation using a uniform urban facet albedo of 0.3. An additional simulation with HTRDR-Urban is made for the representative street canyon geometry.

- For the urban geometries with trees, simulations with HTRDR-Urban, TEB-Classical, and TEB-SPARTACUS are made for direct and diffuse solar radiation using a uniform urban facet albedo of 0.4.

https://doi.org/10.5194/egusphere-2024-1118
Preprint. Discussion started: 24 May 2024

- For all urban geometries, simulations are made for terrestrial radiation using a uniform urban facet emissivity of 0.9. In five sensitivity tests, the skin surface temperature (T_{surf}) of all urban facets including tree leaves is set such that the difference to near-surface air temperature is -10 K, 0 K, 10 K, 20 K, and 30 K respectively.

The uncertainties of the radiative observables are quantified as follows:

- For the direct solar radiation, the simulated radiative observables are displayed as a function of γ for selected urban morphologies. The normalised mean absolute error ($\bar{\Gamma}$, Eq. 18) is defined to quantify the uncertainty of a radiative observable across different values of γ. The uncertainty is defined here as the difference between the TEB observable ($O_{\mathrm{TEB},\gamma}$) and the HTRDR-Urban one ($O_{\mathrm{HTRDR},\gamma}$).

$$\bar{\Gamma} = \frac{\sum_\gamma \dot{Q}_{D,\gamma} |O_{\mathrm{TEB},\gamma} - O_{\mathrm{HTRDR},\gamma}|}{\sum_\gamma \dot{Q}_{D,\gamma}} \tag{18}$$

- For the diffuse solar radiation and the terrestrial infrared radiation, the absolute error (Γ) of the radiative observable is defined as:

$$\Gamma = |O_{\mathrm{TEB}} - O_{\mathrm{HTRDR}}| \tag{19}$$

4 Results

4.1 Direct downwelling solar radiation

4.1.1 Urban morphologies without trees

The radiative observables for the LCZ9 with flat roofs, LCZ2, and LCZ4 morphologies are displayed in Figure 2. For LCZ9 with its low λ_p and λ_w, most of $\dot{Q}_D$ is absorbed by the ground or reflected, except for low values of γ when the walls absorb most of $\dot{Q}_D$. This is captured by TEB-Classical and TEB-SPARTACUS. However, for TEB-Classical, $\dot{Q}_W$ is overestimated and $\dot{Q}_G$ underestimated for γ between 5° and 20°. This is because the infinitely-long street canyon geometry employed by TEB-Classical leads to too low shading of building walls by other buildings (Schoetter et al., 2023). TEB-SPARTACUS almost perfectly corrects this shortcoming of TEB-Classical, because the LCZ9 morphology resembling cubes respects well the SPARTACUS-Urban assumption of the decreasing exponential function for p_{ww} and p_{gw} (Stretton et al., 2022). Similar to the findings of Caliot et al. (2022), the TEB-Classical results are almost identical to the HTRDR-Urban ones for the infinitely-long street canyon, which is due to the analytical solution for the radiosity method under these conditions (vacuum and Lambertian surfaces). For γ below 5°, $\dot{Q}_R$ is underestimated by both TEB-Classical and TEB-SPARTACUS, because with a uniform H_{build}, they cannot represent shading of roofs by higher buildings. This shortcoming of TEB-SPARTACUS could be overcome by introducing a variety of building height at each grid point in TEB.

For the LCZ2 morphology, TEB-Classical overestimates $\dot{Q}_W$ and underestimates $\dot{Q}_G$ for γ between 20° and 75° for the same reason as for LCZ9. This issue is improved by TEB-SPARTACUS, but there remain small biases of $\dot{Q}_W$ and $\dot{Q}_G$, because

https://doi.org/10.5194/egusphere-2024-1118
Preprint. Discussion started: 24 May 2024

the selected LCZ2 morphology with street canyons and building courtyards has p_{ww} and p_{gw} which deviate further from the decreasing exponential function than for the LCZ9 morphology. Pitched roofs lead to an underestimation of $\dot{Q}_R$ for both TEB-Classical and TEB-SPARTACUS, which is the reason for the overestimation of $\dot{Q}_G$ by TEB-SPARTACUS.

For the LCZ4 morphology, TEB-SPARTACUS strongly improves the $\dot{Q}_W$ and $\dot{Q}_G$ observables compared to TEB-Classical for γ above 20°. For lower γ, deficits of TEB-SPARTACUS remain because it does not represent the heterogeneous building height.

https://doi.org/10.5194/egusphere-2024-1118
Preprint. Discussion started: 24 May 2024

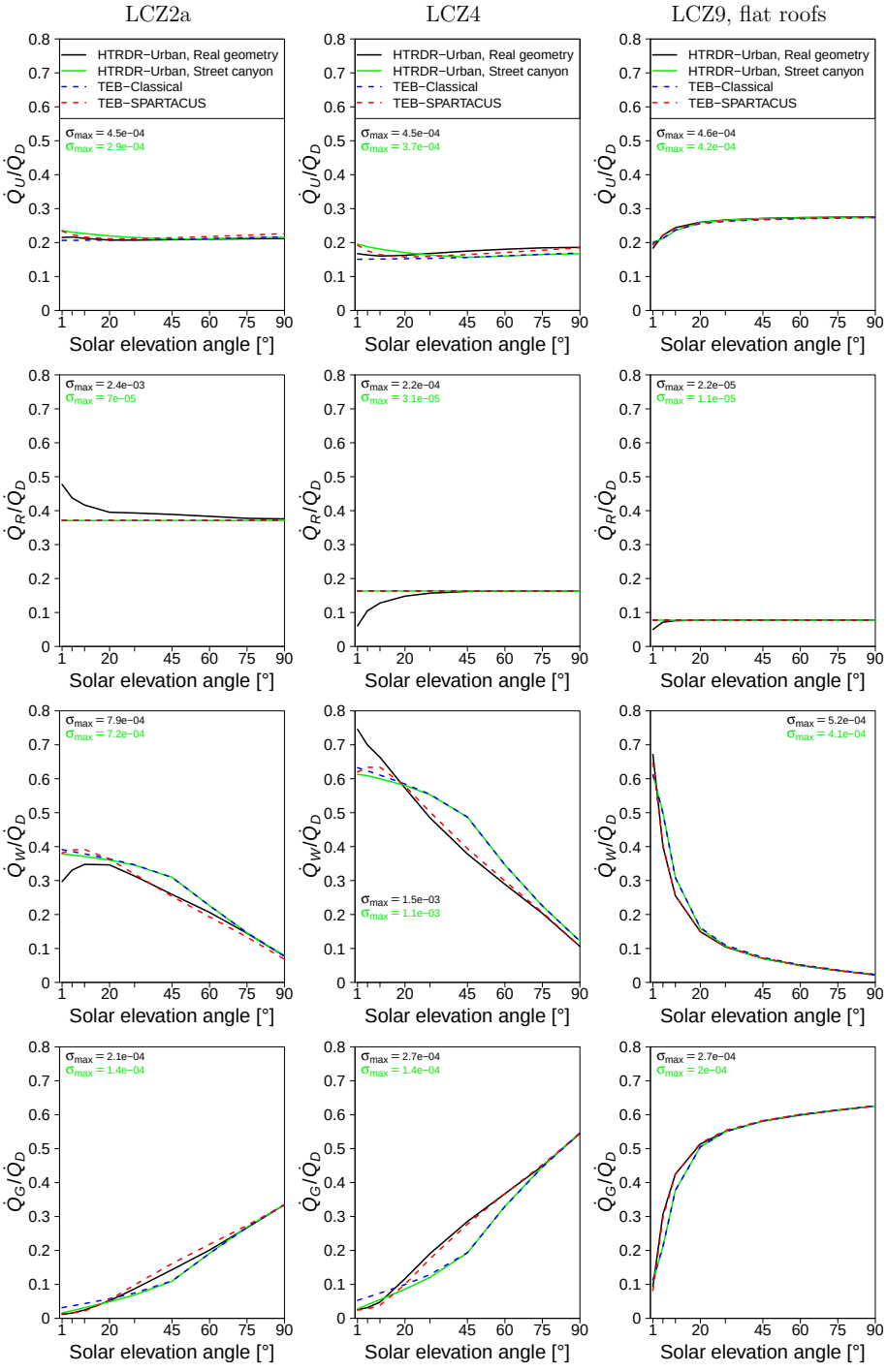

Figure 2. Fraction of downwelling direct solar radiation that is reflected by the city ($\dot{Q}_U$), absorbed by the roofs ($\dot{Q}_R$), the walls ($\dot{Q}_W$), or the ground ($\dot{Q}_G$) simulated by the reference model Monte-Carlo model HTRDR-Urban and the urban canopy model TEB with the Classical and the SPARTACUS-Urban radiation scheme. The values of $\sigma_{\max}$ indicate the maximum value of the standard deviation of the radiative observable obtained from the Monte-Carlo simulations for all values of solar elevation angle.

https://doi.org/10.5194/egusphere-2024-1118
Preprint. Discussion started: 24 May 2024

The $\bar{\Gamma}$ is displayed for all urban morphologies and radiative observables in Figure 3. For both TEB-Classical and TEB-SPARTACUS, the highest $\bar{\Gamma}$ values are found for $\dot{Q}_W$ and $\dot{Q}_G$ whereas $\dot{Q}_U$ and $\dot{Q}_R$ exhibit lower $\bar{\Gamma}$. The $\bar{\Gamma}$ values are highest for the high-rise LCZ1 and LCZ4 morphologies and lowest for the low-rise LCZ3, LCZ6, LCZ8, and LCZ9 morphologies. No difference of $\bar{\Gamma}$ is found for $\dot{Q}_R$, because both TEB-Classical and TEB-SPARTACUS do not consider a variety of building height at each grid point. TEB-SPARTACUS leads to a marked improvement of the other radiative observables for all urban geometries. TEB-SPARTACUS strongly reduces the $\bar{\Gamma}$ for $\dot{Q}_W$ and $\dot{Q}_G$ compared to TEB-Classical for the morphologies with low variability in building height and which resemble blocks. For LCZ1, the $\bar{\Gamma}$ values for $\dot{Q}_W$ and $\dot{Q}_G$ are only slightly reduced, because the strong variety of building height is not considered by TEB-SPARTACUS. For LCZ2a, the $\bar{\Gamma}$ values for $\dot{Q}_W$ and $\dot{Q}_G$ are also only slightly reduced, because this morphology is characterised by street canyons and internal courtyards, which does not perfectly align with the geometrical assumption made by SPARTACUS-Urban. The $\bar{\Gamma}$ values for $\dot{Q}_U$ are strongly reduced for most morphologies, but they are less reduced for LCZ2a and LCZ6a characterised by street canyons and internal courtyards and for LCZ1 with its strong variety in building height.

https://doi.org/10.5194/egusphere-2024-1118
Preprint. Discussion started: 24 May 2024

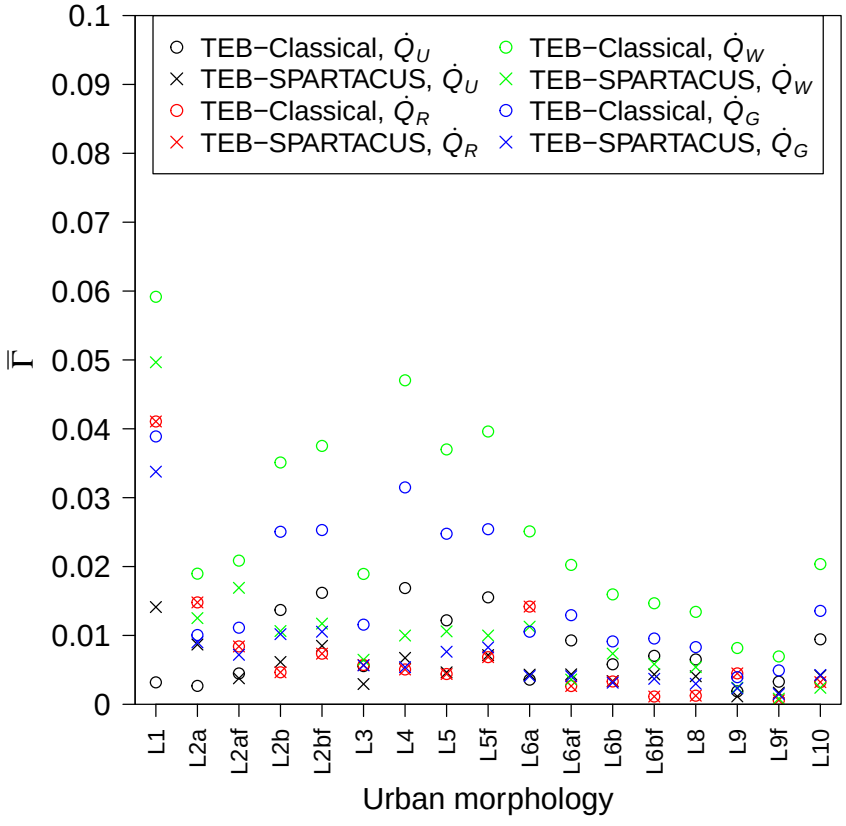

Figure 3. Normalised mean absolute error ($\bar{\Gamma}$, Eq. 18) of the direct solar radiation radiation that is reflected by the city ($\dot{Q}_U$), absorbed by the roofs ($\dot{Q}_R$), the walls ($\dot{Q}_W$), or the ground ($\dot{Q}_G$) when simulated by TEB with the Classical and the SPARTACUS-Urban radiation scheme. The results are shown for all urban morphologies. L1 is LCZ1, L2af is LCZ2a with flat roofs, and so on.

https://doi.org/10.5194/egusphere-2024-1118
Preprint. Discussion started: 24 May 2024

4.1.2 Urban morphologies with trees

Figure 4 displays the solar radiation budget for the LCZ9 district with flat roofs and $10\ \mathrm{m}$ high trees. This district is particular in the way that the trees are rather large ($H_{\mathrm{tree}} = 10\ \mathrm{m}$) compared to the low-rise buildings ($H_{\mathrm{mean}} = 5.9\ \mathrm{m}$). As a consequence, $\frac{\dot{Q}_T}{\dot{Q}_D}$ rises from below 0.1 for γ above $45°$ to above 0.5 for a γ of $1°$. TEB-Classical, which represents the vegetation with a height lower or equal to H_{build} and which consists of a turbid layer filling the entire street canyon between trunk and tree height without taking into account the individual tree borders does not capture the increase of $\dot{Q}_T$ for low values of γ. As a result, $\dot{Q}_T$ is slightly underestimated by TEB-Classical for γ above $45°$ and strongly underestimated for lower γ. TEB-SPARTACUS simulates $\dot{Q}_T$ well. The other terms of the solar radiation budget are also improved with TEB-SPARTACUS compared to TEB-Classical. $\dot{Q}_W$ is considerably reduced for γ below $20°$ with TEB-SPARTACUS due to the enhanced shading of walls by the trees compared with TEB-Classical. $\dot{Q}_G$ is reduced for γ below $60°$ with TEB-SPARTACUS, because there is more shading by trees; it matches better with the reference HTRDR-Urban. $\dot{Q}_U$ is lower for all γ with TEB-SPARTACUS, because there are more multiple reflections of solar radiation leading to a lower probability of reflection towards the sky.

The results for all urban morphologies with trees are displayed in Figure 5. For LCZ5, TEB-SPARTACUS strongly reduces the $\bar{\Gamma}$ values for $\dot{Q}_W$ and $\dot{Q}_G$, whereas for $\dot{Q}_T$ they are only slightly reduced. For $\dot{Q}_R$, there is no difference because the buildings are higher than the trees. The $\bar{\Gamma}$ values for $\dot{Q}_U$ are higher for TEB-SPARTACUS than for TEB-Classical, but this could be due to the fact that for TEB-Classical the $\dot{Q}_U$ is well simulated due to error compensation in other variables. For LCZ4, the $\bar{\Gamma}$ values are lower for all observables, except for $\dot{Q}_R$, for which they remain unchanged. For LCZ2a, the $\dot{Q}_T$ values are low because not much radiation reaches the few trees in this dense mid-rise morphology. For $\dot{Q}_W$, the $\bar{\Gamma}$ values are slightly reduced for TEB-SPARTACUS, but for $\dot{Q}_U$ they are slightly increased.

https://doi.org/10.5194/egusphere-2024-1118
Preprint. Discussion started: 24 May 2024

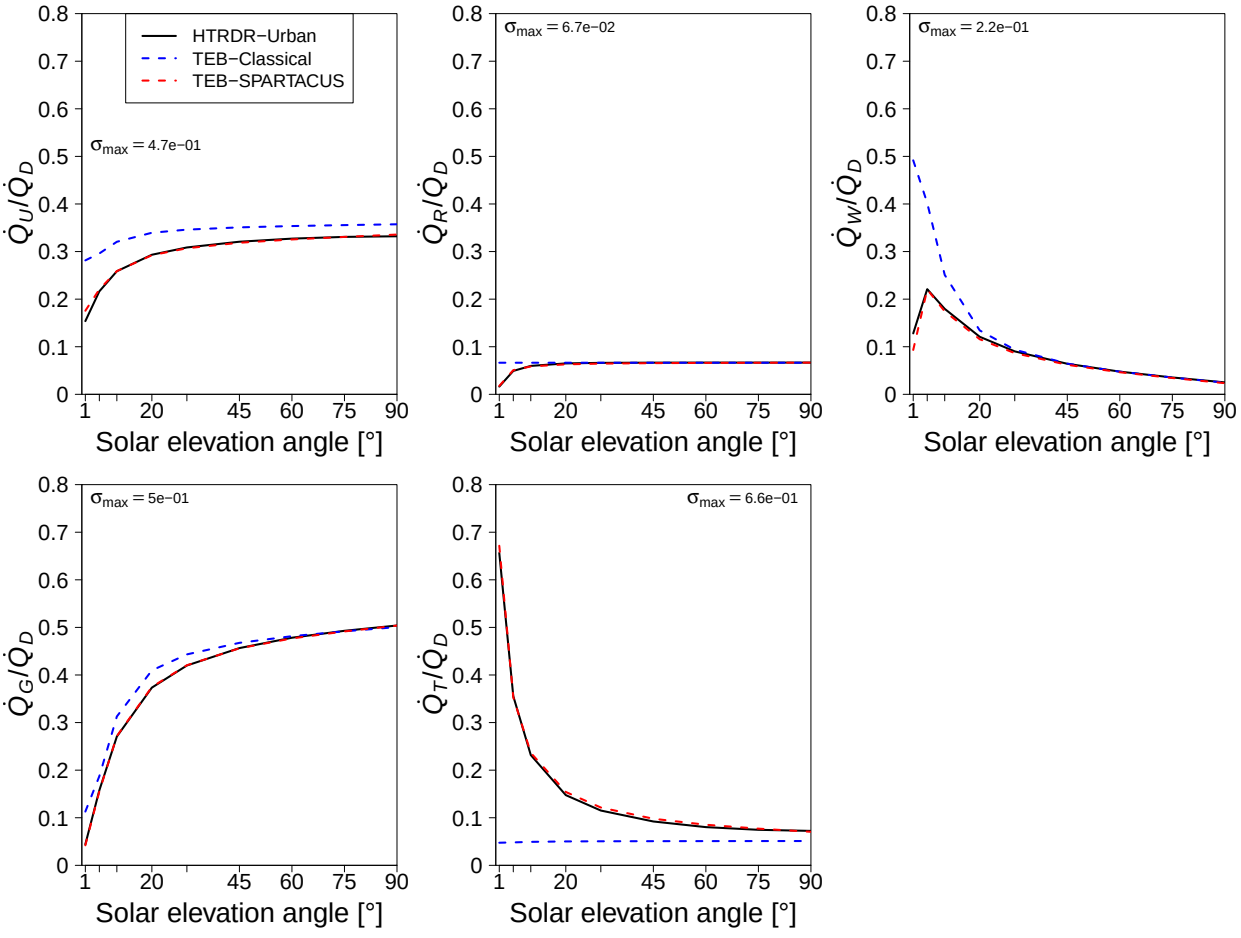

Figure 4. Fraction of direct downwelling solar radiation that is reflected ($\dot{Q}_U$), absorbed by the roofs ($\dot{Q}_R$), the walls ($\dot{Q}_W$), the ground ($\dot{Q}_G$), or urban trees ($\dot{Q}_T$) simulated by the reference model Monte-Carlo model HTRDR-Urban and the urban canopy model TEB with the Classical and the SPARTACUS-Urban radiation scheme for the LCZ9 morphology with trees. The values of $\sigma_{\max}$ indicate the maximum value of the standard deviation of the radiative observable obtained from the Monte-Carlo simulations for all values of solar elevation angle.

https://doi.org/10.5194/egusphere-2024-1118
Preprint. Discussion started: 24 May 2024

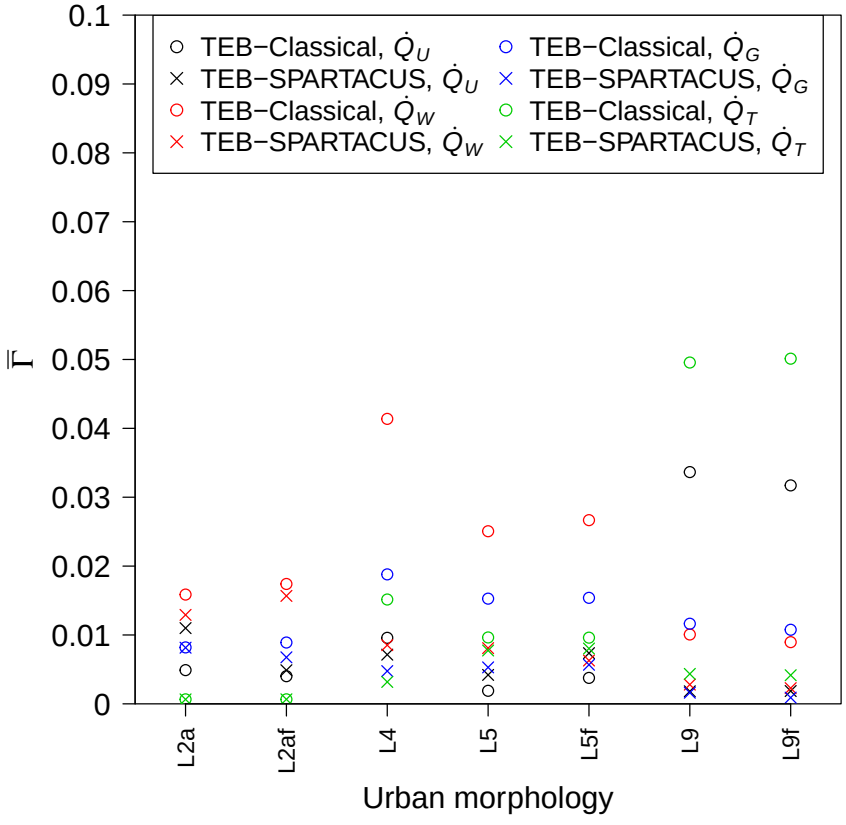

Figure 5. Normalised mean absolute error ($\bar{\Gamma}$, Eq. 18) of the direct solar radiation radiation that is reflected by the city ($\dot{Q}_U$), absorbed by the walls ($\dot{Q}_W$), the ground ($\dot{Q}_G$), or urban trees ($\dot{Q}_T$) when simulated by TEB with the Classical and the SPARTACUS-Urban radiation scheme for all urban morphologies with trees. The results for the direct solar radiation absorbed by the roofs ($\dot{Q}_R$) are not shown, because the differences between TEB-Classical and TEB-SPARTACUS are very small. L2a is LCZ2a, L2af is LCZ2a with flat roofs, and so on.

https://doi.org/10.5194/egusphere-2024-1118
Preprint. Discussion started: 24 May 2024

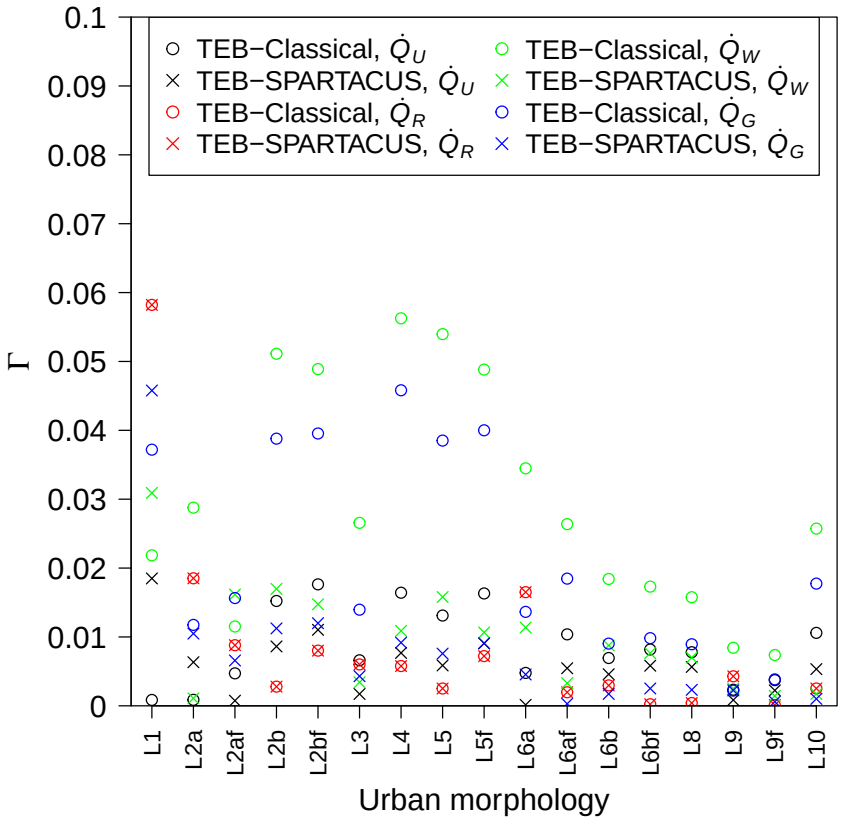

Figure 6. Absolute error (Γ, Eq. 19) of the fraction of diffuse solar radiation that is reflected by the city ($\frac{\dot{Q}_U}{\dot{Q}_D}$), absorbed by the roofs ($\frac{\dot{Q}_R}{\dot{Q}_D}$), the walls ($\frac{\dot{Q}_W}{\dot{Q}_D}$), or the ground ($\frac{\dot{Q}_G}{\dot{Q}_D}$) when simulated by TEB with the Classical and the SPARTACUS-Urban radiation scheme. The results are shown for all urban morphologies. L1 is LCZ1, L2af is LCZ2a with flat roofs, and so on.

4.2 Diffuse downwelling solar radiation

4.2.1 Urban morphologies without trees

For the diffuse downwelling solar radiation, the Γ of the radiative observables $\dot{Q}_U$, $\dot{Q}_R$, $\dot{Q}_W$, and $\dot{Q}_G$ normalised with $\dot{Q}_D$ for TEB-Classical and TEB-SPARTACUS is displayed in Figure 6 for all urban geometries. The results are similar to those for direct downwelling solar radiation. For $\dot{Q}_R$, the Γ values are the same for TEB-Classical and TEB-SPARTACUS because both do not take into account the variety in building height. The Γ values for $\dot{Q}_W$ are strongly reduced for most morphologies, with the exception of LCZ1 and LCZ2a with the flat roofs. The Γ values for $\dot{Q}_G$ and $\dot{Q}_U$ are reduced with TEB-SPARTACUS, except for LCZ1.

https://doi.org/10.5194/egusphere-2024-1118
Preprint. Discussion started: 24 May 2024

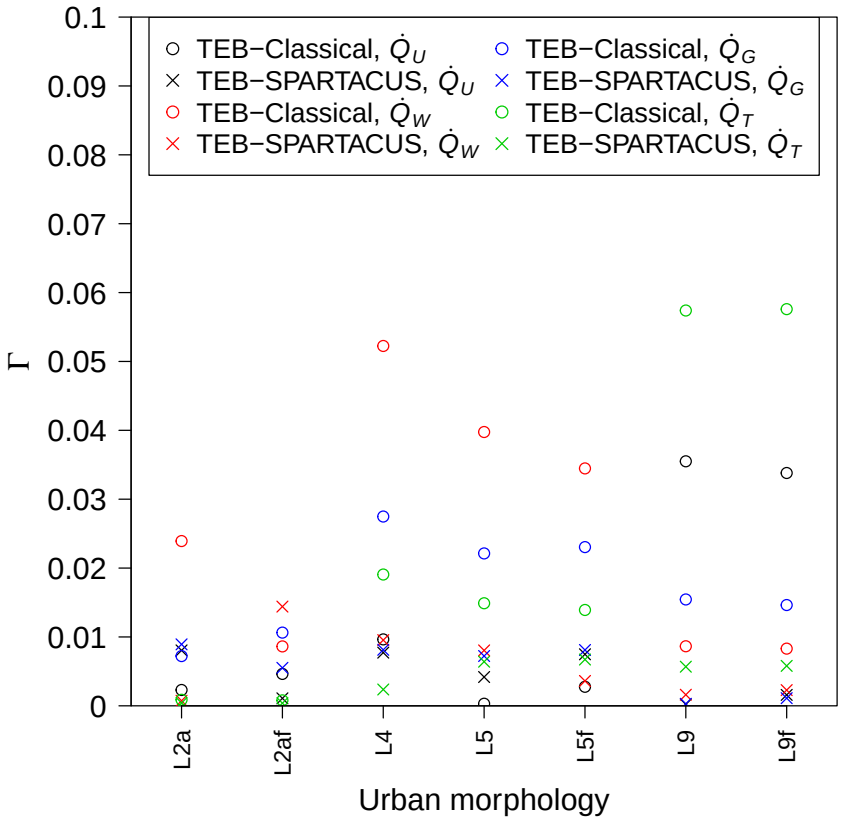

Figure 7. Absolute error (Γ, Eq. 19) of the fraction of diffuse solar radiation that is reflected by the city ($\frac{\dot{Q}_U}{\dot{Q}_D}$), absorbed by the walls ($\frac{\dot{Q}_W}{\dot{Q}_D}$), the ground ($\frac{\dot{Q}_G}{\dot{Q}_D}$), or the urban trees ($\frac{\dot{Q}_T}{\dot{Q}_D}$) when simulated by TEB with the Classical and the SPARTACUS-Urban radiation scheme. The results for the fraction of radiation absorbed by the roofs are not shown, because they differ only little between TEB-Classical and TEB-SPARTACUS. The results are shown for all urban morphologies with trees. L1 is LCZ1, L2af is LCZ2a with flat roofs, and so on.

4.2.2 Urban morphologies with trees

Figure 7 displays the Γ of the radiative observables for diffuse downwelling solar radiation and the urban morphologies with trees. The results are similar to those for direct solar radiation. The Γ values for $\dot{Q}_T$ are strongly reduced with TEB-SPARTACUS, except for LCZ2a for which the trees receive only little solar radiation. The Γ values for $\dot{Q}_R$ remain unchanged for the mid- and high-rise morphologies because the buildings are higher than the trees and slightly increase with TEB-SPARTACUS for LCZ9. The Γ values for $\dot{Q}_W$ are strongly reduced with TEB-SPARTACUS with the notable exception of LCZ2a with tilted roofs. This could be because TEB-Classical gives good results for the wrong reason due to error compensation. The Γ values for $\dot{Q}_G$ are reduced for TEB-SPARTACUS, except for LCZ2a for which they slightly increase. For $\dot{Q}_U$, the results are more mixed, with a reduction of the Γ values for LCZ4 and LCZ9, but an increase for LCZ2a and LCZ5.

https://doi.org/10.5194/egusphere-2024-1118
Preprint. Discussion started: 24 May 2024

4.3 Terrestrial radiation

4.3.1 Urban morphologies without trees

Figure 8 displays the Γ of the radiative observables related to terrestrial radiation for TEB-Classical and TEB-SPARTACUS and the urban morphologies without trees. The Γ values for $\dot{E}_R$ are very small except for LCZ1, because the variability in building height is not considered. There is no difference in the Γ values between TEB-SPARTACUS and TEB-Classical for this observable. For $\dot{E}_W$, the Γ values for TEB-Classical are larger for the mid- and high-rise morphologies and when T_{surf} is higher than the near-surface air temperature. TEB-SPARTACUS reduces the Γ values compared to TEB-Classical for almost all urban morphologies and skin surface temperature values. The improvement due to TEB-SPARTACUS tends to be higher for increasing T_{surf} and the mid- to high-rise urban morphologies. The results for the Γ values of $\dot{E}_G$ are similar to those for $\dot{E}_W$. The TEB-Classical Γ values are highest for the mid- and high-rise morphologies and for higher T_{surf}. TEB-SPARTACUS reduces the Γ values of $\dot{E}_G$ for all urban morphologies and T_{surf} values, except for LCZ1 for which it would be necessary to consider the variety in building height. For the terrestrial radiation exchanged with the sky ($\dot{E}_{\mathrm{sky}}$), the Γ values for TEB-Classical are very small for $T_{\mathrm{surf}} = 284.2$ K and increase for higher values of T_{surf}. TEB-SPARTACUS strongly reduces the Γ values for $\dot{E}_{\mathrm{sky}}$ for all urban morphologies and T_{surf} values.

https://doi.org/10.5194/egusphere-2024-1118
Preprint. Discussion started: 24 May 2024

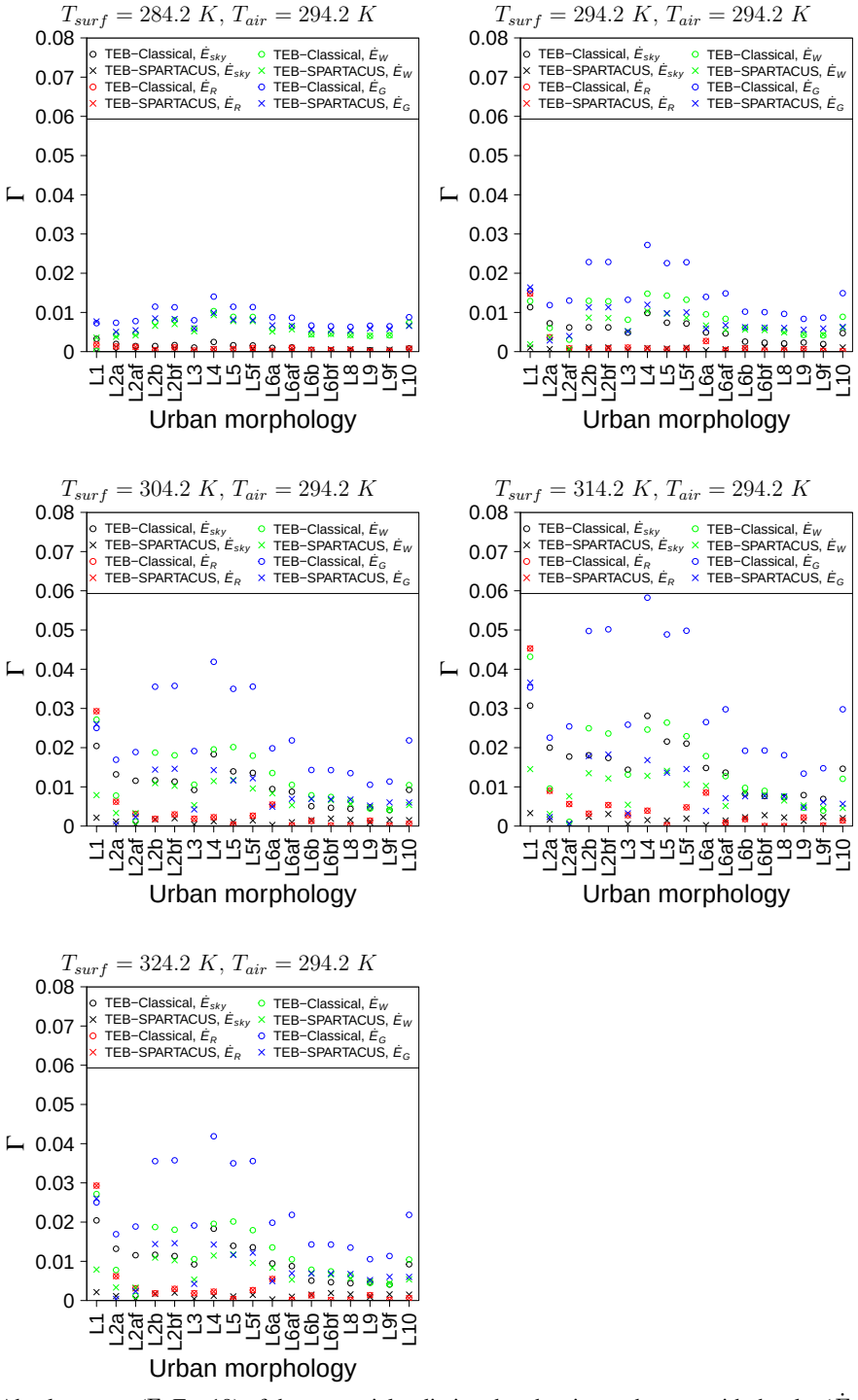

Figure 8. Absolute error (Γ, Eq. 19) of the terrestrial radiation that the city exchanges with the sky ($\dot{E}_{\mathrm{sky}}$) and that is exchanged by the roofs ($\dot{E}_R$), the walls ($\dot{E}_W$), and the ground ($\dot{E}_G$) when simulated by TEB with the Classical and the SPARTACUS-Urban radiation scheme. $\dot{E}_R$ is not shown because its Γ does not differ between TEB-Classical and TEB-SPARTACUS. The results are shown for all urban morphologies. L1 is LCZ1, L2af is LCZ2a with flat roofs, and so on.

https://doi.org/10.5194/egusphere-2024-1118
Preprint. Discussion started: 24 May 2024

4.3.2 Urban morphologies with trees

Figure 9 displays the Γ for the radiative observables related to terrestrial radiation and the urban morphologies with trees. The Γ values for $\dot{E}_T$ are reduced with TEB-SPARTACUS compared to TEB-Classical with the noted exception of LCZ9 with T_{surf} lower than T_{air}. The Γ values for $\dot{E}_F$ are also lower with TEB-SPARTACUS, except for LCZ2a with flat roofs and $T_{\mathrm{surf}} > T_{\mathrm{air}}$. The Γ values for $\dot{E}_G$ are reduced for all urban morphologies except the LCZ9 ones. The Γ values of $\dot{E}_{\mathrm{sky}}$ are strongly reduced for all urban morphologies.

https://doi.org/10.5194/egusphere-2024-1118
Preprint. Discussion started: 24 May 2024

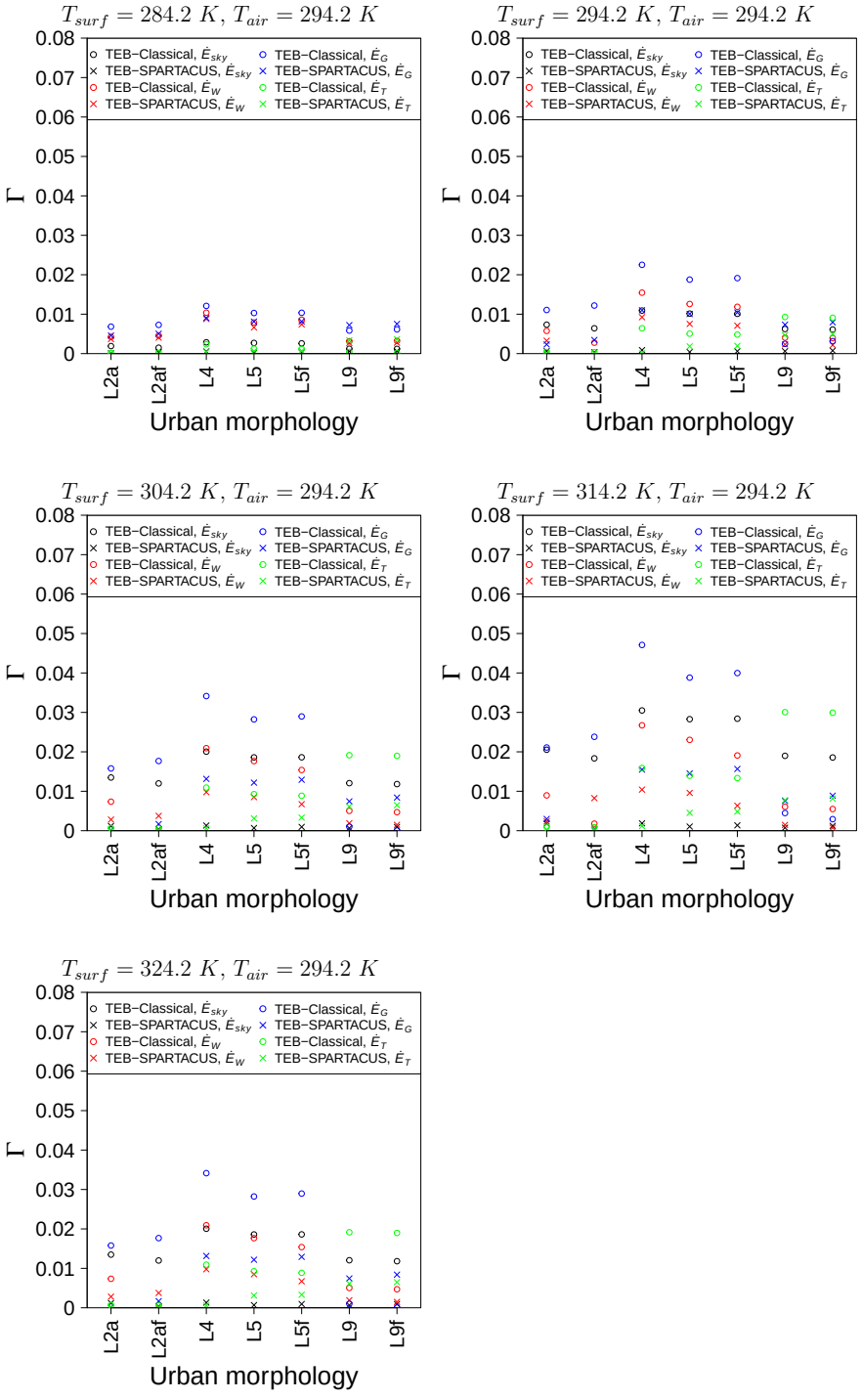

Figure 9. Absolute error (Γ, Eq. 19) of the terrestrial radiation that the city exchanges with the sky ($\dot{E}_{\mathrm{sky}}$) and that is exchanged by the walls ($\dot{E}_W$), the ground ($\dot{E}_G$), and the trees ($\dot{E}_T$) when simulated by TEB with the Classical and the SPARTACUS-Urban radiation scheme. The results are shown for all urban morphologies with trees. L2a is LCZ2a, L2af is LCZ2a with flat roofs, and so on.

https://doi.org/10.5194/egusphere-2024-1118
Preprint. Discussion started: 24 May 2024

5 Discussion

The validation of TEB-SPARTACUS with the Monte-Carlo-based reference model HTRDR-Urban shows improvements of radiative observables related to solar and terrestrial radiation across a variety of urban morphologies. The most relevant findings are:

- TEB-SPARTACUS corrects a main shortcoming of the infinitely-long street canyon assumption made by TEB-Classical that has been documented by Schoetter et al. (2023). This shortcoming consists of too high (too low) absorption of direct solar radiation by the building walls (the ground) due to the wrong distribution of wall-to-wall distances. This improvement can be in the order of 10% of the downwelling direct solar radiation, therefore potentially improving the simulated energy budget of buildings or ground vegetation, and outdoor human thermal comfort.

- For direct downwelling solar radiation and averaged for all solar elevation angles, TEB-SPARTACUS simulates almost all radiative observables with a higher accuracy than TEB-Classical. The improvement can be large (e.g. a factor of 5 less uncertainty) for urban morphologies resembling blocks like LCZ3, LCZ4, LCZ5, LCZ8, LCZ9, and LCZ10. For these morphologies, the decreasing exponential function assumption for the distribution of wall-to-wall and ground-to-wall distances made by SPARTACUS-Urban holds well. However, even for the other morphologies, the radiative observables are more accurately simulated with TEB-SPARTACUS than with TEB-Classical.

- TEB-SPARTACUS strongly improves the solar radiation absorbed by the urban trees because of its representation of trees as cylinders, conserving the tree surface area in contact with air and buildings. This contact area is underestimated by TEB-Classical, which considers the urban trees as a homogeneous turbid layer filling the entire street canyon between trunk and tree height. TEB-SPARTACUS can also represent trees higher than buildings, leading to strong improvements of results for such urban districts. As a result of the improved simulation of the interaction of radiation with urban trees, the other radiative observables are also improved. The improved representation of the radiation absorbed by urban trees could potentially strongly improve the results of simulated evapotranspiration, photosynthesis, or CO_2 uptake by trees.

- Uncertainties of the direct solar radiation observables for low values of solar elevation angle are found with TEB-SPARTACUS for the high-rise districts, which is due to the neglect of the variability of building height. These uncertainties might become more relevant in urban districts with heterogeneous building types, i.e. consisting of a mixture of LCZ. SPARTACUS-Urban is perfectly suited for dealing with such a variety in building height; the TEB geometrical input parameters would have to be modified.

- For the diffuse downwelling solar radiation, the findings are very similar to those for direct downwelling solar radiation when averaging over different values of the solar elevation angle. TEB-SPARTACUS reduces the uncertainties of radiative observables.

- TEB-SPARTACUS leads to a reduction of the uncertainties in simulated radiative observables for terrestrial infrared radiation. The improvement is particularly high when the skin surface temperature is higher than the near-surface air

https://doi.org/10.5194/egusphere-2024-1118
Preprint. Discussion started: 24 May 2024

temperature, which is frequently the case in urban areas. The improvement is found for all urban morphologies except for LCZ1, for which the variety in building height need to be taken into account.

- TEB-SPARTACUS improves the simulation of terrestrial infrared radiation absorbed by urban trees and as a consequence also the other radiative observables in urban districts with trees.

There are several restrictions to the present study.

- Only urban districts with one building type and morphology have been investigated. In real cities, there is frequently a variety of building types in one district, leading for example to a larger variety of building height than in the districts investigated in this study. Since TEB-SPARTACUS does not represent the variety of building height, it might predict radiative observables with lower accurracy in such districts.
- No variety of urban material albedo, emissivity, or skin surface temperature has been investigated. TEB-SPARTACUS might have a different performance for non-homogeneous districts than for the homogeneous ones investigated in this study.
- Only one type of urban tree with homogeneous height and diameter has been investigated. Urban districts with a variety of tree types and tree characteristics should be analysed to investigate whether the results of this study still hold for these.
- In real cities, there are frequently overhanging and pitched roofs. Simulations with HTRDR-Urban (not shown) reveal that such features can strongly change the direct solar radiation budget (e.g. the partitioning between the radiation absorbed by the roofs or the walls). Neither TEB-Classical nor TEB-SPARTACUS represent such features and they have not been included in the validation presented here. The obtained accurracy of radiative observables reported in this study might therefore be too optimistic compared to real cities.

6 Conclusions

The urban canopy model TEB has been coupled with the urban radiation parametrisation SPARTACUS-Urban which assumes a decreasing exponential for the probability density function of the wall-to-wall and ground-to-wall distances. This is more realistic than the assumption of an infinitely-long street canyon employed by the original TEB. While the original TEB employs the radiosity method to calculate the radiative exchanges, SPARTACUS-Urban solves the RTE using the discrete ordinate method. This allows to take into account many additional physical processes like specular reflections, wavelength-dependent albedo of urban materials, and interaction of radiation with the air, aerosols, or fog in the UCL. SPARTACUS-Urban also represents urban trees in a more realistic fashion, notably as cylinders conserving the contact area between trees, air, and building walls.

The TEB-SPARTACUS coupling has been made in a very simple way by conserving the original TEB's geometrical complexity, i.e. there is no variety of building height at each grid point. Furthermore, urban material albedo and emissivities in TEB do still not depend on the wavelength, and atmospheric scattering and absorption is not considered in TEB-SPARTACUS.

https://doi.org/10.5194/egusphere-2024-1118
Preprint. Discussion started: 24 May 2024

The difference between TEB-Classical and TEB-SPARTACUS is therefore only due to the changed assumptions on urban and tree geometry and the replacement of the radiosity method by the discrete ordinate method to calculate the radiative exchanges. TEB-SPARTACUS has been validated using a Monte-Carlo-based reference model (HTRDR-Urban) for procedurally-generated urban morphologies mimicking the Local Climate Zones. The urban morphologies are homogeneous since there is no variety of building type, albedo, emissivity, or skin surface temperature at the scale of the district. A clear improvement compared to TEB-Classical of the key radiative observables, i.e. the direct and diffuse solar, and terrestrial radiation exchanged by the roofs, the walls, the ground, urban trees, and the sky has been found when using TEB-SPARTACUS. This might improve the simulated building energy budget (e.g. the heating and air conditioning energy consumption), outdoor human thermal comfort, urban vegetation evapotranspiration and CO_2 uptake, and even the urban heat island effect.

The next step in the TEB-SPARTACUS development is to consider a variety of building height at each grid point, since this will strongly improve radiative observables in high-rise districts and districts with heterogeneous building height. Also, an atmospheric radiation scheme could be called by TEB-SPARTACUS to calculate the scattering and absorption of radiation in the UCL. This can strongly improve the simulated terrestrial radiation (Hogan, 2019b; Schoetter et al., 2023). Furthermore, TEB-SPARTACUS can be used in urban climate simulations when TEB is coupled with an atmospheric model like Meso-NH (Lac et al., 2018) to investigate its impact on the urban heat island.

Code availability. The software archive on Zenodo (https://zenodo.org/records/11244064) contains the exact model version used in this article, and a user manual describing the TEB-SPARTACUS namelist and how to install the model, run and plot the validation simulations to reproduce the figures in this article. TEB-SPARTACUS is also included in the free and open-source SURFEXv9.0 (http://www.umr-cnrm.fr/surfex/spip.php?article387) that is under a CeCILL-C license.

Author contributions. Robert Schoetter did the TEB and SPARTACUS-Urban coupling, the execution and analysis of the HTRDR-Urban reference simulations, and the majority of the writing. Robin Hogan prepared SPARTACUS-Urban for its coupling with TEB, provided guidance on the use of Monte-Carlo reference simulations for radiative transfer, and supervised the TEB-SPARTACUS validation. Cyril Caliot lead the HTRDR-Urban reference model development and supervised the TEB-SPARTACUS validation. Valéry Masson supervised the TEB-SPARTACUS coupling. All co-authors have read the entire manuscript and helped to improve the original draft.

Competing interests. The authors declare no competing interests

Acknowledgements. Simone Kotthaus is acknowledged for sharing the Spectral Library of Impervious Urban Materials, and Vincent Eymet for his help with the creation of the optical properties files. This work received financial support from the French Agency for Ecological

https://doi.org/10.5194/egusphere-2024-1118
Preprint. Discussion started: 24 May 2024

Transition ADEME (project MODRADURB-1917C001) and from the French National Research Agency through Grant ANR-21-CE46-0013.

https://doi.org/10.5194/egusphere-2024-1118
Preprint. Discussion started: 24 May 2024

References

Blazejczyk, K., Epstein, Y., Jendritzky, G., Staiger, H., and Tinz, B.: Comparison of UTCI to selected thermal indices, Int J Biometeorol, 56, 515–535, https://doi.org/10.1007/s00484-011-0453-2, 2012.

Bueno, B., Pigeon, G., Norford, L. K., Zibouche, K., and Marchadier, C.: Development and evaluation of a building energy model integrated in the TEB scheme, Geosci Model Dev, 5, 433–448, https://doi.org/10.5194/gmd-5-433-2012, 2012.

Caliot, C., Schoetter, R., Forest, V., Eymet, V., and Chung, T.-Y.: Model of Spectral and Directional Radiative Transfer in Complex Urban Canopies with Participating Atmospheres, Boundary-Layer Meteorol, https://doi.org/10.1007/s10546-022-00750-5, 2022.

Coddington, O., Lean, L. J., Doug, L., Pilewskie, P., Snow, M., and NOAA CDR Program: NOAA Climate Data Record (CDR) of Solar Spectral Irradiance (SSI), NRLSSI Version 2. [ssi_v02r01_yearly_s1610_e2020_c20210204.nc], https://doi.org/10.7289/V51J97P6, 2015.

Daniel, M., Lemonsu, A., Déqué, M., Somot, S., Alias, A., and Masson, V.: Benefits of explicit urban parameterization in regional climate modeling to study climate and city interactions, Clim Dyn, 52, 2745–2764, https://doi.org/10.1007/s00382-018-4289-x, 2019.

de Munck, C. S., Lemonsu, A., Bouzouidja, R., Masson, V., and Claverie, R.: The GREENROOF module (v7.3) for modelling green roof hydrological and energetic performances within TEB, Geosci Model Dev, 6, 1941–1960, https://doi.org/10.5194/gmd-6-1941-2013, 2013.

Di Napoli, C., Hogan, R. J., and Pappenberger, F.: Mean radiant temperature from global-scale numerical weather prediction models, International Journal of Biometeorology, 64, 1233–1245, https://doi.org/10.1007/s00484-020-01900-5, 2020.

Dissegna, M. A., Yin, T., Wu, H., Lauret, N., Wei, S., Gastellu-Etchegorry, J.-P., and Grêt-Regamey, A.: Modeling Mean Radiant Temperature Distribution in Urban Landscapes Using DART, Remote Sens, 13, https://doi.org/10.3390/rs13081443, 2021.

El Hafi, M., Blanco, S., Dauchet, J., Fournier, R., Galtier, M., Ibarrart, L., Tregan, J.-M., and Villefranque, N.: Three viewpoints on null-collision Monte Carlo algorithms, J Quant Spectrosc Radiat Transf, 260, 107 402, https://doi.org/https://doi.org/10.1016/j.jqsrt.2020.107402, 2021.

Frayssinet, L., Merlier, L., Kuznik, F., Hubert, J.-L., Milliez, M., and Roux, J.-J.: Modeling the heating and cooling energy demand of urban buildings at city scale, Renew Sust Energ Rev, 81, 2318–2327, https://doi.org/10.1016/j.rser.2017.06.040, 2018.

Fröhlich, D. and Matzarakis, A.: Calculating human thermal comfort and thermal stress in the PALM model system 6.0, Geosci Model Dev, 13, 3055–3065, https://doi.org/10.5194/gmd-13-3055-2020, 2020.

Galtier, M., Blanco, S., Caliot, C., Coustet, C., Dauchet, J., El Hafi, M., Eymet, V., Fournier, R., Gautrais, J., Khuong, A., Piaud, B., and Terrée, G.: Integral formulation of null-collision Monte Carlo algorithms, J Quant Spectrosc Radiat Transf, 125, 57–68, https://doi.org/10.1016/j.jqsrt.2013.04.001, 2013.

Gastellu-Etchegorry, J.-P.: 3D Modeling of satellite spectral images, radiation budget and energy budget of urban landscapes, Meteorol Atmos Phys, MAP-0/939, 1–21, https://doi.org/10.1007/s00703-008-0344-1, 2008.

Gastellu-Etchegorry, J.-P., Yin, T., Lauret, N., Cajgfinger, T., Gregoire, T., Grau, E., Feret, J.-B., Lopes, M., Guilleux, J., Dedieu, G., Malenovský, Z., Cook, B. D., Morton, D., Rubio, J., Durrieu, S., Cazanave, G., Martin, E., and Ristorcelli, T.: Discrete Anisotropic Radiative Transfer (DART 5) for Modeling Airborne and Satellite Spectroradiometer and LIDAR Acquisitions of Natural and Urban Landscapes, Remote Sens, 7, 1667–1701, https://doi.org/10.3390/rs70201667, 2015.

Geletič, J., Lehnert, M., Resler, J., Krč, P., Middel, A., Krayenhoff, E., and Krüger, E.: High-fidelity simulation of the effects of street trees, green roofs and green walls on the distribution of thermal exposure in Prague-Dejvice, Build Environ, 223, 109 484, https://doi.org/https://doi.org/10.1016/j.buildenv.2022.109484, 2022.

https://doi.org/10.5194/egusphere-2024-1118
Preprint. Discussion started: 24 May 2024

Grimmond, C. S. B., Blackett, M., Best, M. J., Barlow, J., Baik, J.-J., Belcher, S. E., Bohnenstengel, S. I., Calmet, I., Chen, F., Dandou, A., Fortuniak, K., Gouvea, M. L., Hamdi, R., Hendry, M., Kawai, T., Kawamoto, Y., Kondo, H., Krayenhoff, E. S., Lee, S.-H., Loridan, T., Martilli, A., Masson, V., Miao, S., Oleson, K., Pigeon, G., Porson, A., Ryu, Y.-H., Salamanca, F., Shashua-Bar, L., Steeneveld, G.-J., Tombrou, M., Voogt, J., Young, D., and Zhang, N.: The International Urban Energy Balance Models Comparison Project: First Results from Phase 1, J Appl Meteorol Clim, 49, 1268–1292, https://doi.org/10.1175/2010JAMC2354.1, 2010.

Grimmond, C. S. B., Blackett, M., Best, M. J., Baik, J.-J., Belcher, S. E., Beringer, J., Bohnenstengel, S. I., Calmet, I., Chen, F., Coutts, A., Dandou, A., Fortuniak, K., Gouvea, M. L., Hamdi, R., Hendry, M., Kanda, M., Kawai, T., Kawamoto, Y., Kondo, H., Krayenhoff, E. S., Lee, S.-H., Loridan, T., Martilli, A., Masson, V., Miao, S., Oleson, K., Ooka, R., Pigeon, G., Porson, A., Ryu, Y.-H., Salamanca, F., Steeneveld, G., Tombrou, M., Voogt, J. A., Young, D. T., and Zhang, N.: Initial results from Phase 2 of the International Urban Energy Balance Model Comparison, Int J Climatol, 31, 244–272, https://doi.org/10.1002/joc.2227, 2011.

Hamdi, R. and Masson, V.: Inclusion of a Drag Approach in the Town Energy Balance (TEB) Scheme: Offline 1D Evaluation in a Street Canyon, J Appl Meteorol Clim, 47, 2627–2644, https://doi.org/10.1175/2008JAMC1865.1, 2008.

Hogan, R. J.: An Exponential Model of Urban Geometry for Use in Radiative Transfer Applications, Boundary-Layer Meteorol, 170, 357–372, https://doi.org/10.1007/s10546-018-0409-8, 2019a.

Hogan, R. J.: Flexible Treatment of Radiative Transfer in Complex Urban Canopies for Use in Weather and Climate Models, Boundary-Layer Meteorol, 173, 53–78, https://doi.org/10.1007/s10546-019-00457-0, 2019b.

Hogan, R. J., Schäfer, S. A. K., Klinger, C., Chiu, J. C., and Mayer, B.: Representing 3-D cloud radiation effects in two-stream schemes: 2. Matrix formulation and broadband evaluation, J Geophys Res Atmos, 121, 8583–8599, https://doi.org/https://doi.org/10.1002/2016JD024875, 2016.

Kotthaus, S., Smith, T., Wooster, M., and Grimmond, S.: Spectral Library of Impervious Urban Materials (Version 1.0) [LUMA_SLUM_SW.csv LUMA_SLUM_IR.csv], http://doi.org/10.5281/zenodo.4263842, 2013.

Kotthaus, S., Smith, T. E., Wooster, M. J., and Grimmond, C.: Derivation of an urban materials spectral library through emittance and reflectance spectroscopy, ISPRS J Photogramm Remote Sens, 94, 194–212, https://doi.org/10.1016/j.isprsjprs.2014.05.005, 2014.

Krayenhoff, E. S., Christen, A., Martilli, A., and Oke, T. R.: A Multi-layer Radiation Model for Urban Neighbourhoods with Trees, Boundary-Layer Meteorol, 151, 139–178, https://doi.org/10.1007/s10546-013-9883-1, 2014.

Kwok, Y. T., Schoetter, R., Lau, K. K.-L., Hidalgo, J., Ren, C., Pigeon, G., and Masson, V.: How well does the local climate zone scheme discern the thermal environment of Toulouse (France)? An analysis using numerical simulation data, Int J Climatol, 0, 1–24, https://doi.org/10.1002/joc.6140, 2019.

Lac, C., Chaboureau, J.-P., Masson, V., Pinty, J.-P., Tulet, P., Escobar, J., Leriche, M., Barthe, C., Aouizerats, B., Augros, C., Aumond, P., Auguste, F., Bechtold, P., Berthet, S., Bielli, S., Bosseur, F., Caumont, O., Cohard, J.-M., Colin, J., Couvreux, F., Cuxart, J., Delautier, G., Dauhut, T., Ducrocq, V., Filippi, J.-B., Gazen, D., Geoffroy, O., Gheusi, F., Honnert, R., Lafore, J.-P., Lebeaupin Brossier, C., Libois, Q., Lunet, T., Mari, C., Maric, T., Mascart, P., Mogé, M., Molinié, G., Nuissier, O., Pantillon, F., Peyrillé, P., Pergaud, J., Perraud, E., Pianezze, J., Redelsperger, J.-L., Ricard, D., Richard, E., Riette, S., Rodier, Q., Schoetter, R., Seyfried, L., Stein, J., Suhre, K., Taufour, M., Thouron, O., Turner, S., Verrelle, A., Vié, B., Visentin, F., Vionnet, V., and Wautelet, P.: Overview of the Meso-NH model version 5.4 and its applications, Geosci Model Dev, 11, 1929–1969, https://doi.org/10.5194/gmd-11-1929-2018, 2018.

Lemonsu, A., Masson, V., Shashua-Bar, L., Erell, E., and Pearlmutter, D.: Inclusion of vegetation in the Town Energy Balance model for modelling urban green areas, Geosci Model Dev, 5, 1377–1393, https://doi.org/10.5194/gmd-5-1377-2012, 2012.

https://doi.org/10.5194/egusphere-2024-1118
Preprint. Discussion started: 24 May 2024

Lemonsu, A., Caillaud, C., Alias, A., Riette, S., Seity, Y., Le Roy, B., Michau, Y., and Lucas-Picher, P.: What added value of CNRM-AROME convection-permitting regional climate model compared to CNRM-ALADIN regional climate model for urban climate studies? Evaluation over Paris area (France), Clim Dyn, 61, 1643–1661, https://doi.org/10.1007/s00382-022-06647-w, 2023.

Lipson, M., Grimmond, S., Best, M., Chow, W. T. L., Christen, A., Chrysoulakis, N., Coutts, A., Crawford, B., Earl, S., Evans, J., Fortuniak, K., Heusinkveld, B. G., Hong, J.-W., Hong, J., Järvi, L., Jo, S., Kim, Y.-H., Kotthaus, S., Lee, K., Masson, V., McFadden, J. P., Michels, O., Pawlak, W., Roth, M., Sugawara, H., Tapper, N., Velasco, E., and Ward, H. C.: Harmonized gap-filled datasets from 20 urban flux tower sites, Earth Syst Sci Data, 14, 5157–5178, https://doi.org/10.5194/essd-14-5157-2022, 2022.

Martilli, A., Clappier, A., and Rotach, M. W.: An Urban Surface Exchange Parameterisation for Mesoscale Models, Boundary-Layer Meteorol, 104, 261–304, https://doi.org/10.1023/A:1016099921195, 2002.

Masson, V.: A Physically-Based Scheme For The Urban Energy Budget In Atmospheric Models, Boundary-Layer Meteorol, 94, 357–397, https://doi.org/10.1023/A:1002463829265, 2000.

Masson, V., Bonhomme, M., Salagnac, J.-L., Briottet, X., and Lemonsu, A.: Solar panels reduce both global warming and urban heat island, Front Environ Sci, 2, 1–10, 2014.

Oke, T. R.: The energetic basis of the urban heat island, Q J R Meteorol Soc, 108, 1–24, https://doi.org/10.1002/qj.49710845502, 1982.

Pigeon, G., Zibouche, K., Bueno, B., Bras, J. L., and Masson, V.: Improving the capabilities of the Town Energy Balance model with up-to-date building energy simulation algorithms: an application to a set of representative buildings in Paris, Energy Build, 76, 1 – 14, https://doi.org/https://doi.org/10.1016/j.enbuild.2013.10.038, 2014.

Redon, E., Lemonsu, A., and Masson, V.: An urban trees parameterization for modeling microclimatic variables and thermal comfort conditions at street level with the Town Energy Balance model (TEB-SURFEX v8.0), Geosci Model Dev, 13, 385–399, https://doi.org/10.5194/gmd-13-385-2020, 2020.

Redon, E. C., Lemonsu, A., Masson, V., Morille, B., and Musy, M.: Implementation of street trees within the solar radiative exchange parameterization of TEB in SURFEX v8.0, Geosci Model Dev, 10, 385–411, https://doi.org/10.5194/gmd-10-385-2017, 2017.

Roth, M.: Review of atmospheric turbulence over cities, Q J R Meteorol Soc, 126, 941–990, https://doi.org/10.1002/qj.49712656409, 2000.

Schoetter, R., Masson, V., Bourgeois, A., Pellegrino, M., and Lévy, J.-P.: Parametrisation of the variety of human behaviour related to building energy consumption in the Town Energy Balance (SURFEX-TEB v.8.2), Geosci Model Dev, 10, 2801–2831, https://doi.org/10.5194/gmd-10-2801-2017, 2017.

Schoetter, R., Kwok, Y. T., de Munck, C., Lau, K. K. L., Wong, W. K., and Masson, V.: Multi-layer coupling between SURFEX-TEB-v9.0 and Meso-NH-v5.3 for modelling the urban climate of high-rise cities, Geosci Model Dev, 13, 5609–5643, https://doi.org/10.5194/gmd-13-5609-2020, 2020.

Schoetter, R., Caliot, C., Chung, T.-Y., Hogan, R. J., and Masson, V.: Quantification of Uncertainties of Radiative Transfer Calculation in Urban Canopy Models, Boundary-Layer Meteorol, https://doi.org/https://doi.org/10.1007/s10546-023-00827-9, 2023.

Schäfer, S. A. K., Hogan, R. J., Klinger, C., Chiu, J. C., and Mayer, B.: Representing 3-D cloud radiation effects in two-stream schemes: 1. Longwave considerations and effective cloud edge length, J Geophys Res Atmos, 121, 8567–8582, https://doi.org/https://doi.org/10.1002/2016JD024876, 2016.

Seity, Y., Brousseau, P., Malardel, S., Hello, G., Bénard, P., Bouttier, F., Lac, C., and Masson, V.: The AROME-France Convective-Scale Operational Model, Mon Weather Rev, 139, 976–991, https://doi.org/10.1175/2010MWR3425.1, 2011.

Stewart, I. D. and Oke, T. R.: Local Climate Zones for Urban Temperature Studies, Bull Am Meteorol Soc, 93, 1879–1900, https://doi.org/10.1175/BAMS-D-11-00019.1, 2012.

https://doi.org/10.5194/egusphere-2024-1118
Preprint. Discussion started: 24 May 2024

Stretton, M. A., Morrison, W., Hogan, R., and Grimmond, S.: Evaluation of the SPARTACUS-Urban radiation model for vertically resolved shortwave radiation in urban areas, Boundary-Layer Meteorol, https://doi.org/10.1007/s10546-022-00706-9, 2022.

Stretton, M. A., Morrison, W., Hogan, R., and Grimmond, S.: Evaluation of vertically resolved longwave radiation in SPARTACUS-Surface 0.7.3 and the sensitivity to urban surface temperatures, EGUsphere, 2023, 1–28, https://doi.org/10.5194/egusphere-2022-1002, 2023.

Strømann-Andersen, J. and Sattrup, P.: The urban canyon and building energy use: Urban density versus daylight and passive solar gains, Energy Buil, 43, 2011–2020, https://doi.org/10.1016/j.enbuild.2011.04.007, 2011.

Thorsson, S., Lindberg, F., Eliasson, I., and Holmer, B.: Different methods for estimating the mean radiant temperature in an outdoor urban setting, Int J Climatol, 27, 1983–1993, https://doi.org/https://doi.org/10.1002/joc.1537, 2007.

Villefranque, N., Fournier, R., Couvreux, F., Blanco, S., Cornet, C., Eymet, V., Forest, V., and Tregan, J.-M.: A Path-Tracing Monte Carlo Library for 3-D Radiative Transfer in Highly Resolved Cloudy Atmospheres, J Adv Model Earth Syst, 11, 2449–2473, https://doi.org/10.1029/2018MS001602, 2019.